Morphology of Monolayer MgO Films on Ag(100): Switching from Corrugated Islands to Extended Flat Terraces

Jagriti Pal,[1,2] Marco Smerieri,[1] Edvige Celasco,[1,2] Letizia Savio,[1,*] Luca Vattuone,[1,2] and Mario Rocca[1,2]
[1]*IMEM-CNR, UOS Genova, Via Dodecaneso 33, 16146 Genova, Italy*
[2]*Dipartimento di Fisica, Università di Genova, Via Dodecaneso 33, 16146 Genova, Italy*
(Received 14 November 2013; published 26 March 2014)

The ability to engineer nearly perfect ultrathin oxide layers, up to the limit of monolayer thickness, is a key issue for nanotechnological applications. Here we face the difficult and important case of ultrathin MgO films on Ag(100), for which no extended and well-ordered layers could thus far be produced in the monolayer limit. We demonstrate that their final morphology depends not only on the usual growth parameters (crystal temperature, metal flux, and oxygen partial pressure), but also on aftergrowth treatments controlling so far neglected thermodynamics constraints. We thus succeed in tuning the shape of the oxide films from irregular, nanometer-sized, monolayer-thick islands to slightly larger, perfectly squared, bilayer islands, to extended monolayers limited apparently only by substrate steps.

DOI: 10.1103/PhysRevLett.112.126102 PACS numbers: 68.55.-a, 68.35.Ja, 68.37.Ef

Oxide-based materials are often used for relevant technological applications in fields such as catalysis, corrosion protection, micro- and nanoelectronics, sensoristics, spintronics, drug delivery, etc. [1]. This justifies the great effort for a complete characterization of such materials [1–9]. Ultrathin oxide films are of utmost importance, since they may show peculiar electronic and chemical properties different from those of the corresponding bulk materials and which are well known to depend on film structure and defectivity [1,6,10–12]. MgO, in particular, has become the focus of intensive research for its role as an interface material [13], with applications, e.g., as a high k dielectric in electronic devices and in magnetic tunnel junctions [14]. Moreover, the simple cubic structure and the small distortion of the MgO layers grown on Mo(100) or Ag(100) make it an ideal model system for the study of electronic and catalytic properties of oxide films and oxide-supported metal nanoclusters [15,16].

In spite of intensive research, however, some very important issues are still unclear. In particular, no uniform, high quality MgO layers suitable to be exploited as substrates for the deposition of further materials (nanoclusters, admolecules, etc.) have been achieved thus far. In the ultrathin limit, the characteristics of MgO layers depend critically on growth parameters; e.g., the stoichiometry is related to O_2 partial pressure and Mg evaporation rate during reactive deposition [17], while the morphology of the MgO islands is determined by the growth temperature (T_g) [18]. In their investigation of MgO ultrathin layers for $373 \leq T_g \leq 673$ K, Ouvrard *et al.* [18] conclude that the optimal growth condition on Ag(100) corresponds to $T_g = 543$ K. The balance between high mobility of Mg and/or MgO and low mobility of Ag atoms leads then to quite regular islands with average dimensions of ~10 nm. However, Shin *et al.* [19] produced a 3 ML thick MgO/Ag(100) film with more than 20 nm wide terraces and very regular borders at $T_g = 773$ K. Discrepancies are also present in the literature for preparations performed under nominally similar conditions. For $450 < T_g < 500$ K, for example, either nearly square islands with nonpolar borders (i.e., aligned along the Ag $\langle 001 \rangle$ direction) [20] or polar borders ($\langle 01-1 \rangle$ direction) [21,22] were reported.

Our previous investigation of ultrathin MgO films, grown according to the preparation method of ref. [23], showed a characteristic dependence of the Fuchs-Kliever mode frequency on film thickness [24] and an enhanced reactivity towards hydroxylation of monolayers with respect to multilayers [25,26]. However, our x-ray photoemission spectroscopy (XPS) results were not fully compatible with those of ref. [23] and STM inspection revealed that the film structure consists of irregular islands with borders preferentially oriented along $\langle 001 \rangle$ (see ref. [17] and Fig. 1a). Another open issue concerns the height of MgO islands, a quantity only rarely stated explicitly. Some studies report island profiles and effective MgO coverage compatible with a single MgO layer [20], others with bilayers [18,21].

In this Letter we characterize submonolayer MgO films grown by reactive deposition on Ag(100) using different preparation protocols and considering, for the first time, post-deposition treatments. The morphology of the films is analyzed by STM, while their chemical composition is determined by XPS. The analysis of vibrational modes, performed with HREELS, also provides information on the film structure [24]. In addition to the already established influence of T_g on growth mode [18], we find an unexpected dependence of the film morphology on the cooling process after deposition. This parameter is indeed the key issue leading to very uniform layers. Surprisingly, it has been disregarded so far, in spite of its poor reproducibility

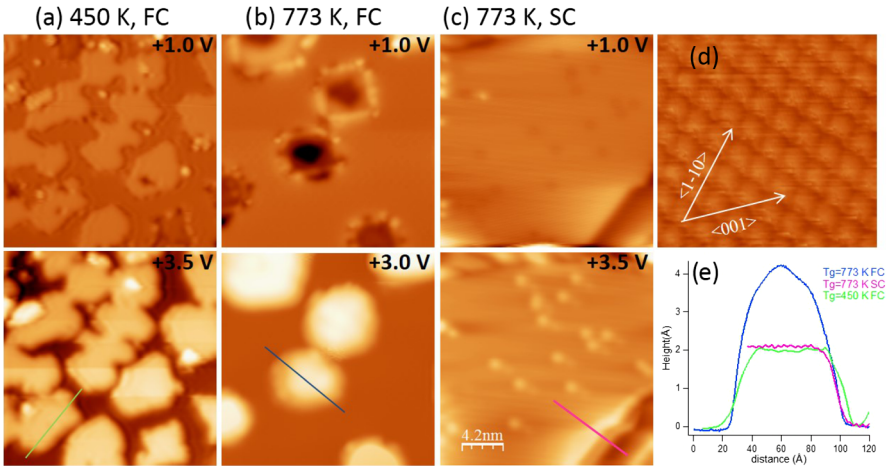

FIG. 1 (color online). (a)–(c), top and bottom: STM Images of MgO films of 0.7 ML nominal thickness grown under different conditions. (a) $T_g = 450$ K, FC; (b) $T_g = 773$ K, FC; (c) $T_g = 773$ K, SC. For all panels, image size 21×21 nm^2, $I = 0.2$ nA. (d) Atomically resolved image of clean Ag(100), used for calibration. High symmetry directions are marked by arrows. Image size 2.4×2.4 nm^2, $V = 0.1$, $I = 0.2$ nA. (e) Height profiles of the different MgO structures cut along the lines marked in the bottom panels of (a)–(c) ($\langle 001 \rangle$ direction, topographic conditions).

due to the strong dependence on the design of the experimental setup.

Experiments were performed in the two ultrahigh vacuum chambers described in the Supplemental Material [27] and equipped for STM and for HREELS and XPS analysis, respectively. In both setups the sample temperature can be varied from $T = 90$ K to $T = 900$ K. Very close cooling rates were set for STM and XPS experiments (see Supplemental Material [27]) to allow for a fair comparison of the data. MgO films of 0.7 ML nominal thickness were grown by reactive deposition at $T_g = 773$ K and $T_g = 450$ K on a Ag(100) single crystal (see Supplemental Material [27]).

STM images were acquired at $T = 77$ K, in constant current mode and with typical tunnelling currents $I = 0.2$ nA and bias voltage applied to the sample $-4.0 < V < +4.0$ V. STM analysis is performed with WSXM software [28].

HREEL spectra were recorded in-specular, at an angle of incidence of the impinging electrons of 62°, with a primary electron energy $E_e = 4.0$ eV and with typical resolution of 4.0 meV. The spectra are normalized to the Wallis mode intensity, weakly dependent on surface preparation. XPS spectra were recorded at normal emission, using the $\mathrm{Al_{k\alpha}}$ excitation source. The binding energy is calibrated fixing the Ag$3d_{5/2}$ line at $\mathrm{E}_b = 368.25$ eV [26,29]. Spectra are normalized to the secondary electron background and fitted with a Gaussian-Lorentz curve and a Shirley background (see Supplemental Material [27]). A relative error of $\pm 5\%$ is estimated for each fit.

Figure 1 reports STM images of three MgO films grown following different protocols. Two different bias voltages are shown for each preparation: $V \geq 3.0$ V corresponds to tunnelling into the conduction band of MgO, thus reaching topographic imaging; on the contrary, $V = 1.0$ V, i.e., tunneling through the MgO band gap, allows better imaging of the details of island borders. For film (a) we adopted the preparation method of Refs. [17,23,25,30]: after flashing the crystal to 720 K, we grew the film at $T_g = 450$ K. The sample was then abruptly cooled below 200 K and inserted into the STM (fast cooling procedure (FC), see Supplemental Material [27]). In preparation (b) we annealed the clean Ag(100) crystal to 850 K to increase surface order and raised the growth temperature up to $T_g = 773$ K. The film was eventually rapidly cooled to $T < 200$ K for STM analysis. Finally, film (c) was obtained with $T_g = 773$ K and slowly cooling (SC) the sample to 250 K before quenching it to $T < 200$ K. The SC procedure requires more than 40 min, instead of the 5 min typical of FC. The different growth protocols lead to films of very different morphologies. Preparation (a) generates MgO islands with irregular borders and average linear dimensions of a few nanometers. Protocol (b) produces cubic islands with $\langle 001 \rangle$ borders and slightly larger average dimensions. The effect of the increased growth temperature is thus readily identified with an enhanced regularity of the islands shape and a reduced defectivity of their borders. The apparent height of the MgO islands in (a) and (b) (top and bottom) shows a strong bias dependence due to the insulating nature of the oxide. At low bias voltage (top row), the islands show well-defined borders and the presence of an internal structure. Under topographic conditions ($V \geq 3.0$ V) the height of the islands is compatible with a single and a double MgO layer for preparations (a) and (b), respectively [Fig. 1(e)]. This is coherent with both the different island density corresponding to the same nominal coverage observed in panels (a) and (b) and the contrasting results in the literature. Indeed, in Ref. [18] it is

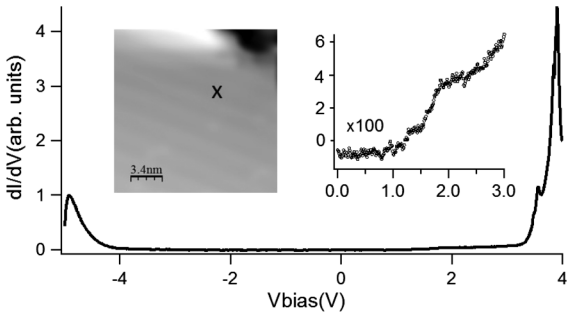

FIG. 2. dI/dV spectrum of the MgO film of preparation (c), recorded at the point marked in the left-hand inset (image size 17×17 nm^2, $V = 1.0$ V, $I = 0.2$ nA) and showing the gap around the Fermi level. Right-hand inset: Enlargement of the spectrum highlighting the presence of an Ag state around 1.8 V.

reported that a maximum of 53% of the Ag (100) surface is covered by MgO islands at a nominal MgO coverage of 1 ML, while Schintke *et al.* [20] show island heights of 2.1 Å, i.e. 1 ML.

The film morphology obtained in preparation (c) is dramatically different from the previous ones, since it shows very large MgO(100) terraces, extending over tens of nanometers and separated by monoatomic steps [see Figs. 1(e) and S2 in the Supplemental Material [27]). Scanning tunnelling spectroscopy (STS) analysis of film (c) (Fig. 2) evidences the gap around the Fermi level and confirms the insulating nature of the surface. This result is related to the combination of high T_g *and* SC. The cooling rate, therefore, plays a pivotal, and so far neglected, role in determining the final product, passing from the equilibrium condition at high T (bilayer) to the formation of extended monolayer islands that maximize the Ag/MgO interface area.

The 0.7 ML MgO films of Fig. 1 were further characterized by integrated spectroscopies. Figure 3 shows the O1s and Mg1s core level spectra of films grown at $T_g = 450$ and 773 K and subject to FC and SC procedures. Spectra marked as (a)–(c) correspond to films (a)–(c) of Fig. 1, respectively. Different preparation methods lead to different spectroscopic signatures. In particular, both E_b(O1s) and E_b(Mg1s) are significantly up-shifted for bilayer islands ($T_g = 773$ K and FC). In all other cases, $E_b(\mathrm{O1}s) < 530$ eV and $E_b(\mathrm{Mg1}s) \leq 1303.5$ eV. This is in agreement with previous literature [9,31] and is justified by the different number of nearest neighbors of atoms in monolayer and bilayer films. Hence, the combination of photoemission and STM data demonstrates that the O1s and Mg1s binding energies and the surface morphology are correlated. Best fits of the XPS intensities (see Supplemental Material [27]) further support this conclusion. The areas of the Mg1s photoemission peaks reported in Fig. 3 (see Table I, column 2), proportional to the relative amount of MgO on the surface, are all compatible with each other, the smallest value (preparation at $T_g = 450$ K and SC) being 70% of the largest one ($T_g = 450$ K and FC). Analysis of the O1s signal (Table I, column 3), which is generally less reliable being possibly affected by the aging processes and/or by a small water/OH contamination, leads to similar results. We conclude, therefore, that a comparable MgO coverage is present on the Ag(100) surface following the different preparation protocols. This is a further, independent proof that the extended terraces of Fig. 1(c) are indeed MgO monolayers. Table I, column 4 reports the stoichiometry of the MgO films, calculated from the ratio of the O1s and Mg1s areas taking into account the different ionization cross sections [32] and the analyzer transmission function [33]. The films grown at $T_g = 450$ K show a nearly unitary stoichiometry. The others have some extra oxygen, which must, therefore, accumulate in the Ag(100) subsurface region [34] and/or at the MgO/Ag(100) interface, possibly forming an

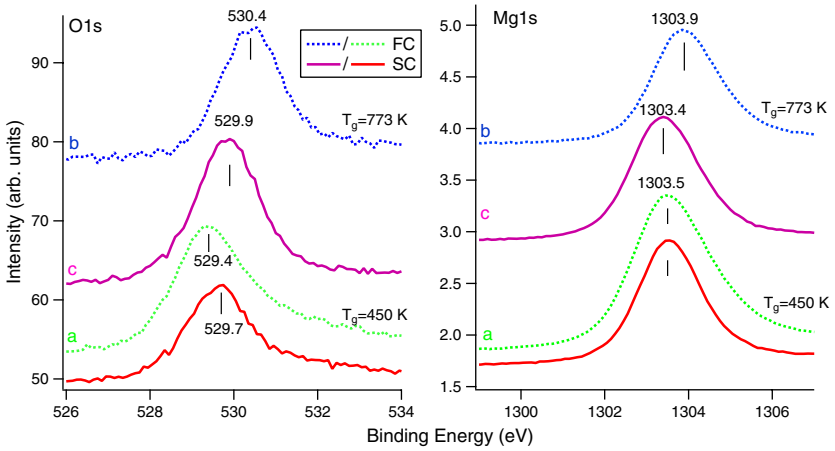

FIG. 3 (color online). O1s and Mg1s photoemission spectra corresponding to 0.7 ML MgO films grown following different protocols. Spectra (a), (b), and (c) correspond to preparations of Fig. 1 with the same labels. Traces were scaled on the secondary electron background of the bottom spectrum and then rigidly up-shifted for a better visualization.

TABLE I. Peak areas and calculated stoichiometry of the 0.7 ML films of Fig. 3.

Preparation T_g—cooling mode	Area Mg(1s) (cps·eV)	Area O(1s) (cps·eV)	Film stoichiometry (O/Mg)
450 K—FC—(a)	138 700	8500	1.22 ± 0.12
450 K—SC	96 300	5700	1.19 ± 0.12
773 K—FC—(b)	98 500	6650	1.34 ± 0.13
773 K—SC—(c)	110 400	7900	1.39 ± 0.14

AgO_x-like compound ($x < 1$). This process is favored at higher T_g. Incorporation of Mg atoms at the buried MgO/Ag(100) interface was recently observed upon additional exposure of the film to Mg flux [13]. Such Mg atoms are responsible for changes in the work function and in the density of states of the oxide. In the present case the main effect of interface O, bigger than Mg and with opposite charge, is probably to expand the substrate lattice and reduce the mismatch between oxide and substrate.

Figure 4 shows the HREEL analysis performed on the same 0.7 ML MgO films of Fig. 3. The bottom spectra refer to films grown at 450 K and subject to the FC (green trace) or SC (red trace) process; top spectra are recorded after producing the films at $T_g = 773$ K (blue trace, FC; purple trace, SC). The spectra are characterized by three intense losses between 50 and 85 meV [(best resolved in the green-dashed spectrum corresponding to preparation (a)].

(1) The 53 meV vibration is intense in preparation (a) ($T_g = 450$ K and FC), significantly reduced for $T_g = 450$ K and SC, and almost absent for films grown at higher T_g. In Ref. [24] it was identified with the microscopic vibration of oxygen atoms at the edges of MgO islands and in contact with the Ag substrate. Here we substantiate this assignment, since comparison with the STM images of Fig. 1 indicates that film (a) corresponds to the conditions in which the fraction of border MgO groups in contact with the metal substrate is maximum.

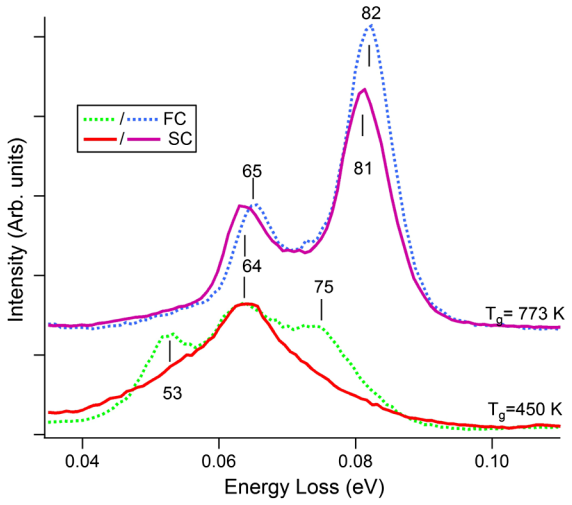

FIG. 4 (color online). HREEL spectra of the 0.7 ML MgO films grown following the different protocols described in the text. Bottom spectra, $T_g = 450$ K; top spectra, $T_g = 773$ K (up-shifted for sake of clarity).

(2) The loss at 64–65 meV is ascribed to the Wallis mode, i.e., the perpendicular motion of oxygen atoms at the topmost layer, by comparison with previous results on MgO bulk [35] and thin films [24,36]. The loss up-shifts by 1 meV when passing from monolayer to bilayer islands [24], as observed also for MnO/Pt(111) [37].

(3) The assignment of the high-energy mode is more delicate, since the macroscopic Fuchs-Kliever mode (i.e., the counterphase vibration of O and Mg sublattices) should be present only for multilayer islands [24,37]. The 82 meV energy loss recorded for film (b) and the weak intensity at this energy in the $T_g = 450$ K and SC spectrum fit perfectly with theory [24]. The losses at 75 meV [film (a)] and at 81 meV [film (c)], on the contrary, must have a different nature. The latter is observed for a superstoichiometric film. One possibility is, therefore, that the additional oxygen atoms at the interface simulate an incomplete second layer and generate a Fuchs-Kliever–like motion of slightly lower energy and reduced intensity. The mode at 75 meV is intense only for the irregular islands of film (a). In Ref. [24] a mode was observed around 71 meV. We suggest, therefore, that modes exist in the 70–75 meV range, the exact frequency depending on the different local environments within the island.

The morphology of MgO films thus depends not only on growth parameters but also on the cooling rate after growth. This result can be rationalized considering that the surface energy of MgO(100) and of Ag(100) is 1.15 J/m^2 [38] and 1.20 J/m^2 [39], respectively. Since the relative difference is $<5\%$, we expect the entropic term to determine the growth mode, provided that the deposition rate is low and the diffusion rate high enough to get rid of kinetic effects. When the temperature of the film is rapidly quenched from 773 K to $T < 450$ K, the morphology observed is the one thermodynamically favored at $T_g = 773$ K. On the other hand, when the entropic term is negligible, thermodynamics favors complete substrate wetting, i.e., layer-by-layer growth (Frank–Van der Merve). Therefore, it is reasonable that bilayers are observed for $T_g = 773$ K and FC, because then we expect a significant amount of 3D growth under equilibrium conditions (Volmer-Weber growth). On the contrary, if the system has time to relax, the bilayers evolve into single layers while cooling down. Therefore, for $T_g = 450$ K monolayer islands form and for $T_g = 773$ K and SC nearly perfect MgO monolayers are observed. SC is essential in this respect to ensure that the required mobility is present sufficiently long to allow the transition from bilayer to monolayer to be completed.

In conclusion, we demonstrate that different growth protocols, including both deposition conditions and the

so far neglected after-growth treatments, lead to very different morphologies of oxide films. The combination of these parameters can be relevant not only for the production of oxide thin films but also for many other layered systems. Since the film structure influences both chemical and electronic properties [1,10,12] of the layers, a full control of all experimental parameters opens important perspectives for applications in catalysis and for the use of ultrathin oxide films as support for the further deposition of organic and inorganic nano-objects.

The authors thank A. Orzelli for participating in the initial stage of STM experiments and Compagnia S. Paolo for funding. J. P. acknowledges support from ICTP through a postdoctoral grant.

*Corresponding author.
savio@fisica.unige.it

[1] G. Pacchioni and H. J. Freund, Chem. Rev. **113**, 4035 (2013).
[2] C. T. Campbell, Surf. Sci. Rep. **27**, 1 (1997).
[3] X. Liu, C. Chen, Y. Zhao, and B. Jia, J. Nanomater. **2013**, 736375.(2013).
[4] A. I. Braginsky, J. R. Gavaler, M. A. Janocko, and J. Talvacchio, *Superconducting Quantum Interference Devices and their Applications* (Walter de Gruyter, Berlin, 1985).
[5] D. Panda and T. Y. Tseng, Thin Solid Films **531**, 1 (2013).
[6] G. Pacchioni, Chem. Eur. J. **18**, 10144 (2012).
[7] L. Giordano and G. Pacchioni, Acc. Chem. Res. **44**, 1244 (2011).
[8] S. A. Chambers, Adv. Mater. **22**, 219 (2010).
[9] C. J. Nelin, P. S. Bagus, M. A. Brown, M. Sterrer, and H. J. Freund, Angew. Chem. **123**, 10356 (2011).
[10] C. Freysoldt, P. Rinke, and M. Scheffler, Phys. Rev. Lett. **99**, 086101 (2007).
[11] H. J. Freund, H. Kuhlenbeck, and V. Staemmler, Rep. Prog. Phys. **59**, 283 (1996).
[12] F. P. Netzer, F. Allegretti, and S. Surnev, J. Vac. Sci. Technol. B **28**, 1 (2010).
[13] T. Jaouen, S. Tricot, G. Delhaye, B. Lépine, D. Sébilleau, G. Jézéquel, and P. Schieffer, Phys. Rev. Lett. **111**, 027601 (2013).
[14] C. Tusche, H. Meyerheim, N. Jedrecy, G. Renaud, A. Ernst, J. Henk, P. Bruno, and J. Kirschner, Phys. Rev. Lett. **95**, 176101 (2005).
[15] G. Barcaro and A. Fortunelli, J. Chem. Theory Comput. **1**, 972 (2005).
[16] A. K. Santra and D. W. Goodman, J. Phys. Condens. Matter **15**, R31 (2003).
[17] G. Cabailh, R. Lazzari, H. Cruguel, J. Jupille, L. Savio, M. Smerieri, A. Orzelli, L. Vattuone, and M. Rocca, J. Phys. Chem. A **115**, 7161 (2011).
[18] A. Ouvrard, J. Niebauer, A. Ghalgaoui, C. Barth, C. R. Henry, and B. Bourguignon, J. Phys. Chem. C **115**, 8034 (2011).
[19] H.-J. Shin, J. Jung, K. Motobayashi, S. Yanagisawa, Y. Morikawa, Y. Kim, and M. Kawai, Nat. Mater. **9**, 442 (2010).
[20] S. Schintke, S. Messerli, M. Pivetta, F. Patthey, L. Libioulle, M. Stengel, A. De Vita, and Wolf-Dieter Schneider, Phys. Rev. Lett. **87**, 276801 (2001); S. Schintke and W. D. Schneider, J. Phys. Condens. Matter **16**, R49 (2004).
[21] S. Valeri, S. Altieri, U. del Pennino, A. di Bona, P. Luches, and A. Rota, Phys. Rev. B **65**, 245410 (2002).
[22] A. M. Ferrari, S. Casassa, C. Pisani, S. Altieri, A. Rota, and S. Valeri, Surf. Sci. **588**, 160 (2005).
[23] S. Altieri, L. H. Tjeng, and G. A. Sawatzky, Phys. Rev. B **61**, 16948 (2000).
[24] L. Savio, E. Celasco, L. Vattuone, M. Rocca, and P. Senet, Phys. Rev. B **67**, 075420 (2003).
[25] L. Savio, E. Celasco, L. Vattuone, and M. Rocca, J. Chem. Phys. **119**, 12053 (2003).
[26] L. Savio, E. Celasco, L. Vattuone, and M. Rocca, J. Phys. Chem. B **108**, 7771 (2004).
[27] See Supplemental Material at http://link.aps.org/supplemental/10.1103/PhysRevLett.112.126102 for (1) experimental details, including the growth methodology of MgO films, (2) the cooling rate of the samples during FC and SC, (3) the extended monolayer films, and (4) the analysis of XPS peaks.
[28] I. Horcas, R. Fernández, J. M. Gómez-Rodríguez, J. Colchero, J. Gómez-Herrero, and A. M. Baro, Rev. Sci. Instrum. **78**, 013705 (2007).
[29] C. J. Powell, Appl. Surf. Sci. **89**, 141 (1995).
[30] L. Savio, M. Smerieri, A. Orzelli, L. Vattuone, M. Rocca, F. Finocchi, and J. Jupille, Surf. Sci. **604**, 252 (2010).
[31] S. Altieri, L. H. Tjeng, F. C. Voogt, T. Hibma, and G. A. Sawatzky, Phys. Rev. B **59**, R2517 (1999).
[32] J. H. Scofield, J. Electron Spectrosc. Relat. Phenom. **8**, 129 (1976).
[33] P. Ruffieux, P. Schwaller, O. Gröning, L. Schlapbach, P. Gröning, Q. C. Herd, D. Funnemann, and J. Westermann, Rev. Sci. Instrum. **71**, 3634 (2000).
[34] M. Rocca *et al.*, Phys. Rev. B **63**, 081404(R) (2001).
[35] C. Oshima, T. Aizawa, R. Souda, and Y. Ishizawa, Solid State Commun. **73**, 731 (1990).
[36] Y. Hwang, R. Souda, T. Aizawa, W. Hayami, S. Otani, and Y. Ishizawa, Jpn. J. Appl. Phys. **36**, 5707 (1997).
[37] S. Sachert, S. Polzin, K. Kostov, and W. Widdra, Phys. Rev. B **81**, 195424 (2010).
[38] A. Gibson, R. Haydock, and J. P. LaFemina, J. Vac. Sci. Technol. A **10**, 2361 (1992).
[39] H. L. Skriver and N. M. Rosengaard, Phys. Rev. B **46**, 7157 (1992).